

# Towards a method for detecting the potential genotoxicity of nanomaterials



Deliverable 4.4: Determination of specific surface area of  
NANOGENOTOX nanomaterials

Final report

Key intrinsic physicochemical characteristics of  
NANOGENOTOX nanomaterials

May  
2012

*This document arises from the NANOGENOTOX Joint Action which has received funding from the European Union, in the framework of the Health Programme under Grant Agreement n°2009 21.  
This publication reflects only the author's views and the Community is not liable for any use that may be made of the information contained therein.*



Co-funded by  
the Health Programme  
of the European Union



Grant Agreement n° 2009 21 01

---

## WP 4 : Physicochemical Characterization of Manufactured Nanomaterials (MNs) and Exposure Media (EMs)

### Deliverable 4.4: Determination of specific surface area of NANOGENOTOX nanomaterials

---

Deliverable leader: NRCWE

Keld Alstrup Jensen

The National Research Centre for the Working Environment (NRCWE),

Lersø Parkallé 105, DK-2100 Copenhagen, DENMARK



National Research Centre  
for the Working Environment



<b>Workflow</b>	
<b>Author(s)</b>	<b>Reviewer(s)</b>
Camille Guiot and Olivier Spalla (CEA)	WP Leader: Keld Alstrup Jensen (NRCWE)
Rosica Nikolova and Boris Shivachev (IMC-BAS)	Coordinator: Nathalie Thieriet (ANSES)
Keld Alstrup Jensen (NRCWE)	

Document status:	v.1.0	draft	Creation date:	9/01/2012
	v.1.1	final draft	Creation date:	8/03/2012
	v.1.2	revised and reviewed by KAJ	Creation date:	31/05/2012
	v.1.3	revised by coordination team	Creation date	11/02/2013
	v.1.4	revised and reviewed by authors	Creation date	19/02/2013

Confidentiality level of the deliverable		
<b>PU</b>	Public	PU
<b>CO</b>	Confidential, only for members of the consortium (including the Commission Services)	

<b>1</b>	<b>INTRODUCTION .....</b>	<b>4</b>
<b>2</b>	<b>NANOMATERIALS AND INFORMATION GIVEN BY SUPPLIERS .....</b>	<b>5</b>
<b>3</b>	<b>METHODS.....</b>	<b>7</b>
3.1	SMALL-ANGLE X-RAY SCATTERING (SAXS).....	7
3.1.1	SAXS measurements.....	7
3.1.2	Raw data treatment and calculations.....	7
3.2	BRÜNAUER, EMMETT AND TELLER (BET).....	7
3.2.1	Measurement and data treatment .....	8
3.2.2	Observations on use and applicability.....	8
<b>4</b>	<b>RESULTS .....</b>	<b>10</b>
4.1	SAXS.....	10
4.1.1	TiO <sub>2</sub> nanomaterials (NM10X) .....	10
4.1.2	SiO <sub>2</sub> nanomaterials (NM20X).....	13
4.1.3	CNT nanomaterials (NM40X) .....	16
4.2	BET.....	21
4.2.1	TiO <sub>2</sub> (NM10X).....	22
4.2.2	Synthetic Amorphous Silica (NM20#) .....	22
4.2.3	Carbon nanotubes (NM40#).....	22
<b>5</b>	<b>DISCUSSION.....</b>	<b>26</b>
5.1	COMPARISON OF SAXS AND BET DATA OBTAINED FROM THE PROJECT .....	26
5.2	COMPARISON BETWEEN BET DATA OBTAINED FROM THE PROJECT AND BET DATA FROM PRODUCERS.....	28
<b>6</b>	<b>CONCLUSIONS .....</b>	<b>30</b>
	<b>REFERENCES .....</b>	<b>31</b>
	<b>APPENDIX A: STANDARD OPERATION PROCEDURES .....</b>	<b>32</b>
	SAXS SAMPLE PREPARATION .....	32
	BET SAMPLE PREPARATION AND APPARATUS SPECIFICATION .....	33
	<b>A.2. REMINDER ON THE TECHNIQUE AND GENERAL LAWS.....</b>	<b>35</b>
	SAXS EXPERIMENT .....	35
	BET MEASUREMENT .....	38



# 1 Introduction

Three major nanomaterial (NM) properties are hypothesized to govern human health and environmental impacts, and thus, are of the highest priority for the production, characterization, testing, and modification. These are (1) their morphology and structure, (2) their interfacial properties, and (3) their physical-chemical reactivity. Physical morphology and chemical structure govern initial miscibility, stability, and reactivity of NMs in the suspending media of interest. These early interactions, ultimately, give rise to NM interfacial properties that control aggregation, transport, deposition, and partitioning behavior in aqueous media. Finally, the combination of bulk and interfacial NM properties define long-term stability, reactivity, and fate in biological and environmental systems. Consequently, for material characteristics and assessment of potential relations to NM hazards, determination of the surface area, pore size, and porosity are some of the most critical physico-chemical end-points.

The widely used Brünauer, Emmett and Teller (BET) method was used for estimating surface area together with the less classical Small Angle X-ray Scattering (SAXS). Procedures using transmission electron microscopy also exists. In the Joint Actions project, NANOGENOTOX (funded by the EAHC (Executive Agency for Health and Consumers), we only applied SAXS and BET.

This report describes in detail the final surface area data from the NANOGENOTOX project. The report also contains in-depth description and evaluation of the SOPs applied and developed for the analysis. The report officially fulfills a part of the initial Deliverable 4 and Milestone 1 of WP4 in the Joint Actions project. Temporary results and SOPs have previously been reported in Guiot et al (2010) and Jensen et al., (2010) as well as in power point presentations at the three General Assembly meetings in Rome (September 2010), Nancy (April 2011) and Copenhagen (October 2011), respectively.

The complete report series on physico-chemical characterization are listed hereafter:

D4.1: Summary report on primary physicochemical properties of manufactured nanomaterials used in NANOGENOTOX

D4.2: Transmission electron microscopic characterization of NANOGENOTOX nanomaterials

D4.3: Crystallite size, mineralogical and chemical purity of NANOGENOTOX nanomaterials

D4.4: Determination of specific surface area of NANOGENOTOX nanomaterials

D4.5: Surface charge, hydrodynamic size and size distributions by zetametry, dynamic light scattering (DLS) and small-angle X-ray scattering (SAXS) in optimum aqueous suspensions for titanium and silicon dioxide

D4.6: Dustiness of NANOGENOTOX nanomaterials using the NRCWE small rotating drum and the INRS Vortex shaker

D4.7: Hydrochemical reactivity, solubility, and biodurability of NANOGENOTOX MN.

## 2 Nanomaterials and information given by suppliers

The tested NANOGENOTOX materials include 6 titania-based products, 5 synthetic amorphous silica products and 6 multi-walled carbon nanotubes (Table 1). Synthetic Amorphous Silica NMs is denoted SAS or SiO<sub>2</sub> in accord with a decision in the NANOGENOTOX Consortium. However, amorphous silica usually is oxygen deficient and may contain other elements and is therefore not SiO<sub>2</sub> *senso stricto*. For titania- and carbon nanotube-based NM, the short used forms are TiO<sub>2</sub> and CNT or MWCNT (Multi-walled CNT).

Table 1. Nanomaterials included in the NANOGENOTOX project and information given by suppliers.

JRC Code	Special notes	Phase	application	Purity wt%	Particle size	BET (m <sup>2</sup> /g)	impurity / coating
NM-100	Dry-milled	anatase	paper loadings, rubber, cosmetics, adhesives, low cost interior paints	98.5	200-220 nm	-	-
NM-101		anatase	semiconductor catalyst for use in photocatalytic processes	91(99)*	< 10 nm	>250	9%*
NM-102		anatase	photocatalytic	95	-	90	-
NM-103	hydrophobic	rutile	cosmetics (sun care, colour), pharma, food	89	20 nm	60	Al <sub>2</sub> O <sub>3</sub> 6%, silicone - Dimethicone 2%
NM-104	hydrophilic	rutile		90	20 nm	60	Al <sub>2</sub> O <sub>3</sub> 6% - Dimethicone 2%
NM-105		rutile/anatase	catalysis, heat stabilizer	-	21 nm	50+/-15	-
NM-200	precipitated	PR-A-02	food, processing	-	15 um	220	10 SiO <sub>2</sub> 1 H <sub>2</sub> O, 2% soluble salts
NM-201	precipitated	PR-B-01	reinforcement, mechanical and optical properties and process	-	-	160	10 SiO <sub>2</sub> 1 H <sub>2</sub> O, 1,5% soluble salts
NM-202	thermal	PY-AB-03	inks, adhesives, cosmetics, reinforcement, powder process, food, pharmaceuticals	>99,8	-	170-230	-
NM-203	thermal	PY-A-04	food, cosmetics pharma, reinforcement	-	12 nm	200+/-25	hydrates?
NM-204	Precipitated		food	-	-	140	-

JRC Code	Special notes	Phase	application	Purity wt%	CNT tube length	BET (m <sup>2</sup> /g)	impurity / coating
NM-400	CCVD <sup>€</sup>	MWCNT	structural composite and energy applications	-	~1.5 um long	250-300	10 wt% oxides/coated with pyrogenic carbon
NM-401	CCVD <sup>€</sup>	MWCNT	structural composite and energy applications	-	5-15 um long	40-300	~2% amorph. carbon
NM-402	CCVD <sup>€</sup>	MWCNT	structural composite and energy applications	-	0.1-10 um long	-	<10 wt%
NM-403	CCVD <sup>€</sup>	MWCNT	structural composite and energy applications	-	1->10 µm long	-	-
NRCWE-006	CCVD <sup>€</sup>	MWCNT	energy / Li-ion battery	>99.5	segments; 3-5 um long	24-28	
NRCWE-007	CCVD <sup>€</sup>	MWCNT	structural composites etc.	-	8-15 nm OD; 10-50 um long	233	ca. 3.2 wt% C impurities/ < 1.5wt% ash (Al, Cl, S)

\* calcination causes loss of 9 wt% and the residual is 99% pure

<sup>€</sup> CCVD : Catalytic Chemical Vapour Deposition

## 3 Methods

The specific surface area of a powder may be determined in different ways. In WP4, two techniques were used to determine the specific surface area of nanomaterials: 1) the typical nitrogen adsorption procedure following the Brünauer Emmet and Teller adsorption method (called the BET method) undertaken by IMC-BAS (Bulgaria), and 2) Small Angle X-ray Scattering (SAXS) on powders achieved by CEA (France). BET-data on NRCWE-006 and NRCWE-007 were kindly provided by NRCWE and the FP7 Nanodevice project in order to complete the Nanogenotox database<sup>1</sup>. The two SOPs are fully described in appendix and in the previous deliverable dedicated to SOP.

### 3.1 *Small-angle X-Ray Scattering (SAXS)*

The raw powders were directly used and inserted into cell for measurement without any treatment, as described by [2]. In appendix, SOPs and a reminder the on SAXS technique, general laws and treatment and calculation have been described.

#### 3.1.1 SAXS measurements

For each sample, two SAXS measurements were performed, one with a short acquisition time to prevent saturation of the detector, typically 200 s or 150 s for TiO<sub>2</sub> and SiO<sub>2</sub> and 60 s for CNT, and one with a long time of acquisition of 1800 s to lower the signal/noise ratio at high q.

#### 3.1.2 Raw data treatment and calculations

Image treatment and calculations on radial averaged data are described in the SOP report [1] for SAXS and USAXS data. Basically, it includes normalization of intensity by parameters of the experiments such as acquisition time, sample thickness, calibration constants determined using reference samples and background subtraction. SAXS data obtained for short time and long time are then concatenated, together with USAXS data to get continuous diffractograms on the whole q range.

### 3.2 *Brünauer, Emmett and Teller (BET)*

The raw powders were directly used without any treatment, as described in appendix. SOPs and a reminder the on BET technique, general laws and treatment and calculation have been described.

---

<sup>1</sup> Data obtained in the EU FP7 NANODEVICE project as a commercial service from QUANTACHROME GmbH & Co. KG ([6] Birkedal et al., 2012)

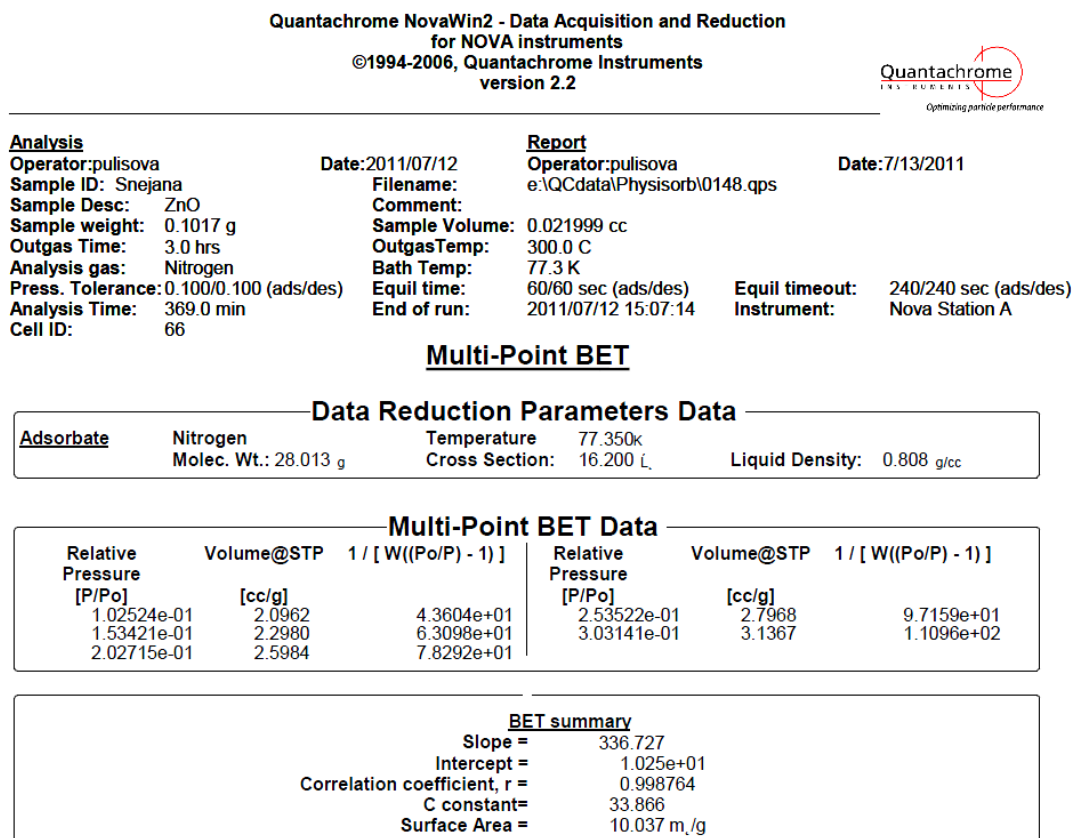
### 3.2.1 Measurement and data treatment

The time of acquisition necessary for BET experiment depends on the sample properties. For each NANOGENOTOX samples, two measurements were performed. All experiment parameters are monitored and recorded on PC providing data reprinting, archiving, graphic overlays and other features. Typical setup parameters and results output are listed below. In order to obtain accurate results the correlation coefficient should be greater than 0.999.

A typical graphical and text output of the BET measurement is shown below for the ZnO samples (Figure 3.1).

### 3.2.2 Observations on use and applicability

The protocol has been tested on all NANOGENOTOX samples. The data are comparable to the producers provided values when available.



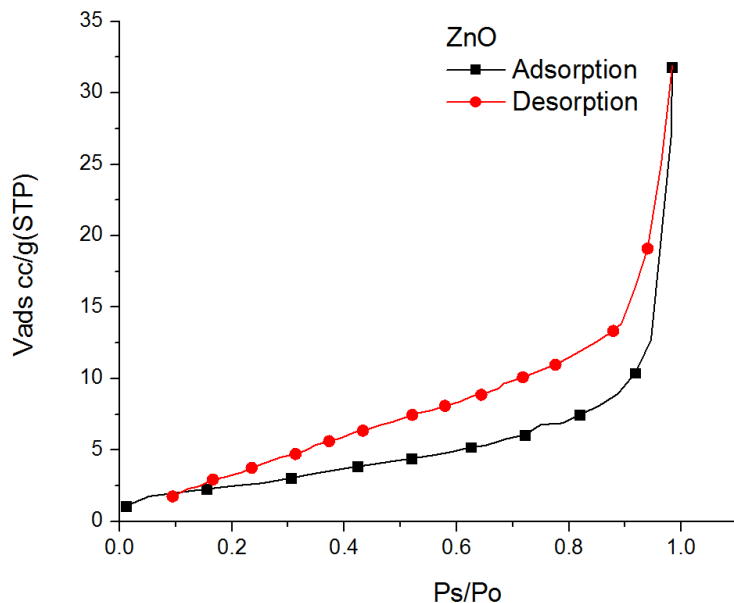


Figure 3.1. Isotherms of nitrogen sorption experiments at 77K for ZnO (Surface area 10m/g) and typical data summary output

## 4 Results

The following chapter summarizes the results from the SAXS and BET analysis, respectively. A comparison between the results obtained by the two methods is made in the discussion, Chapter 5.

### 4.1 SAXS

#### 4.1.1 $\text{TiO}_2$ nanomaterials (NM10X)

All SAXS diffractograms and the corresponding representations in  $I(q)q^4$  for  $\text{TiO}_2$  NM powders are displayed in Figure 4.1, 4.2 and 4.3. Figure 4.2 shows the  $I(q)q^4$  representation and Porod's plateaus raw-plots for each of the  $\text{TiO}_2$  NM.

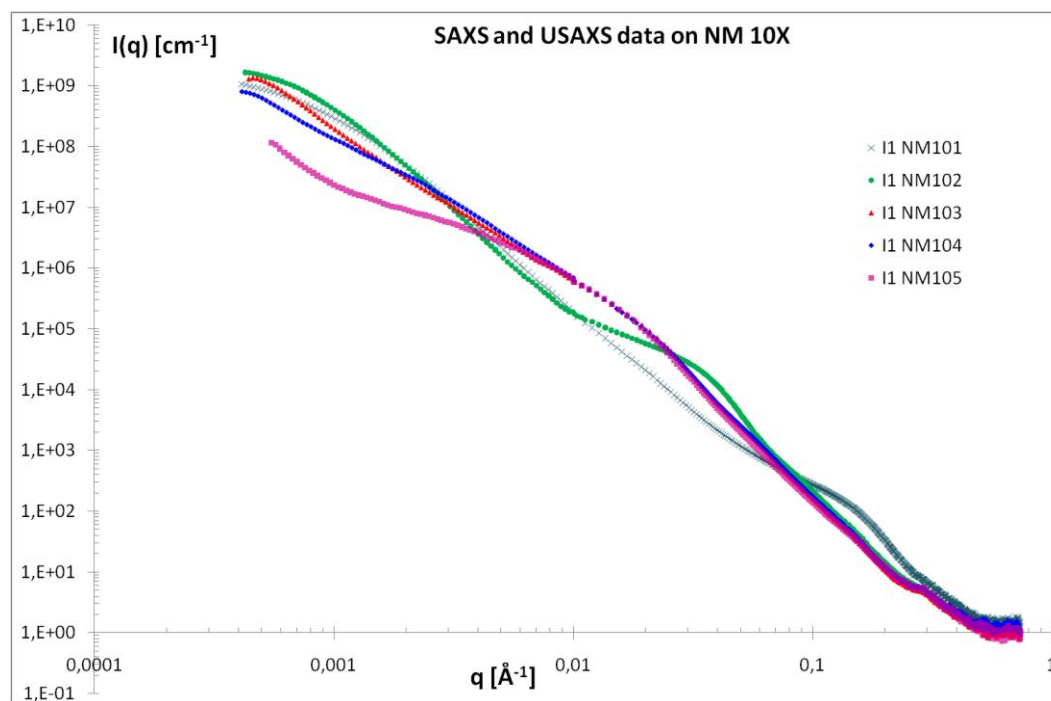


Figure 4.1: SAXS and USAXS results for  $\text{TiO}_2$  raw powders NM101 (blue crosses), NM102 (green circles), NM103 (red triangles), NM104 (blue diamonds) and NM105 (pink square).

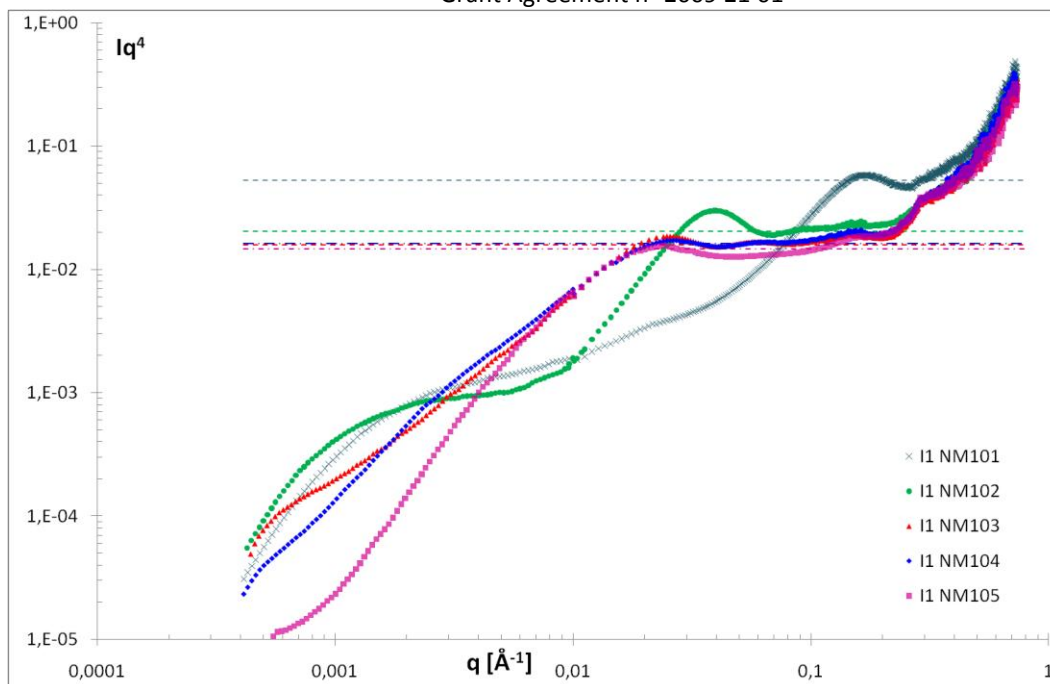
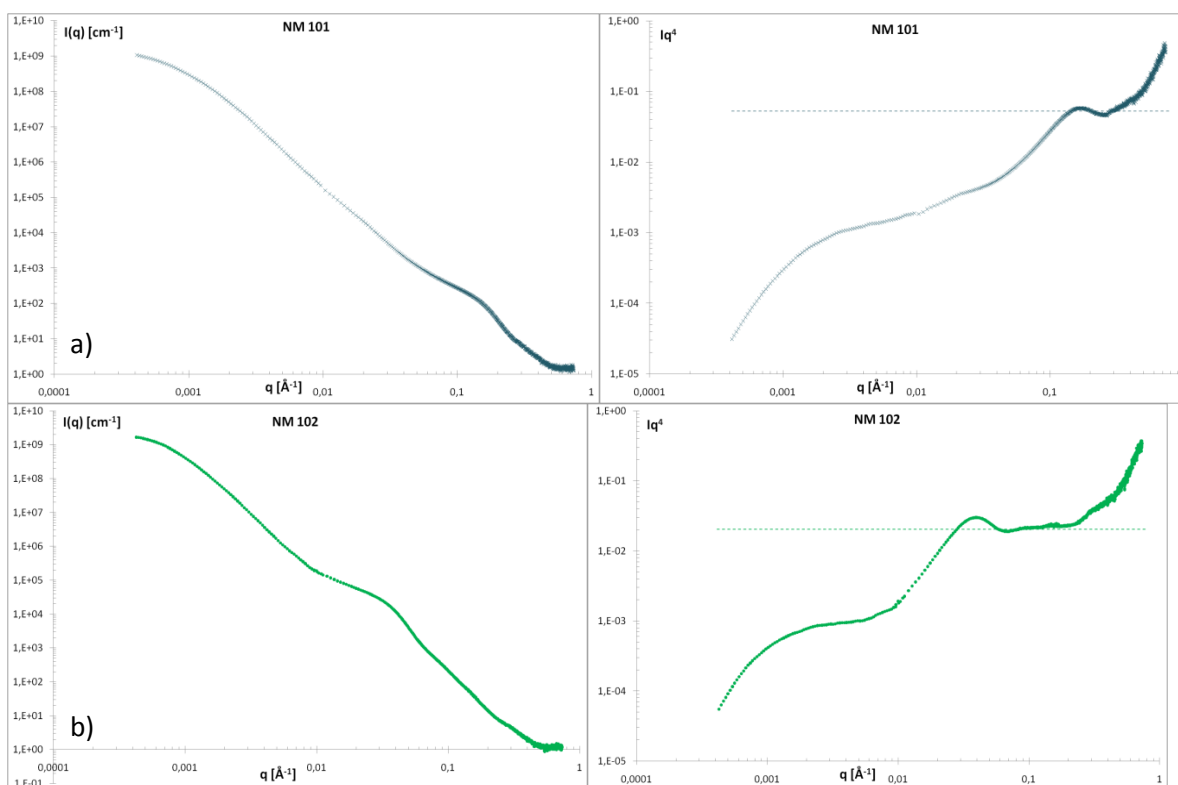


Figure 4.2: Representation in  $Iq^4$  of SAXS and USAXS results of NM101 (blue crosses), NM102 (green circles), NM103 (red triangles), NM104 (blue diamonds) and NM105 (pink squares). The dotted lines are the corresponding Porod's plateaus.



Continued on next page

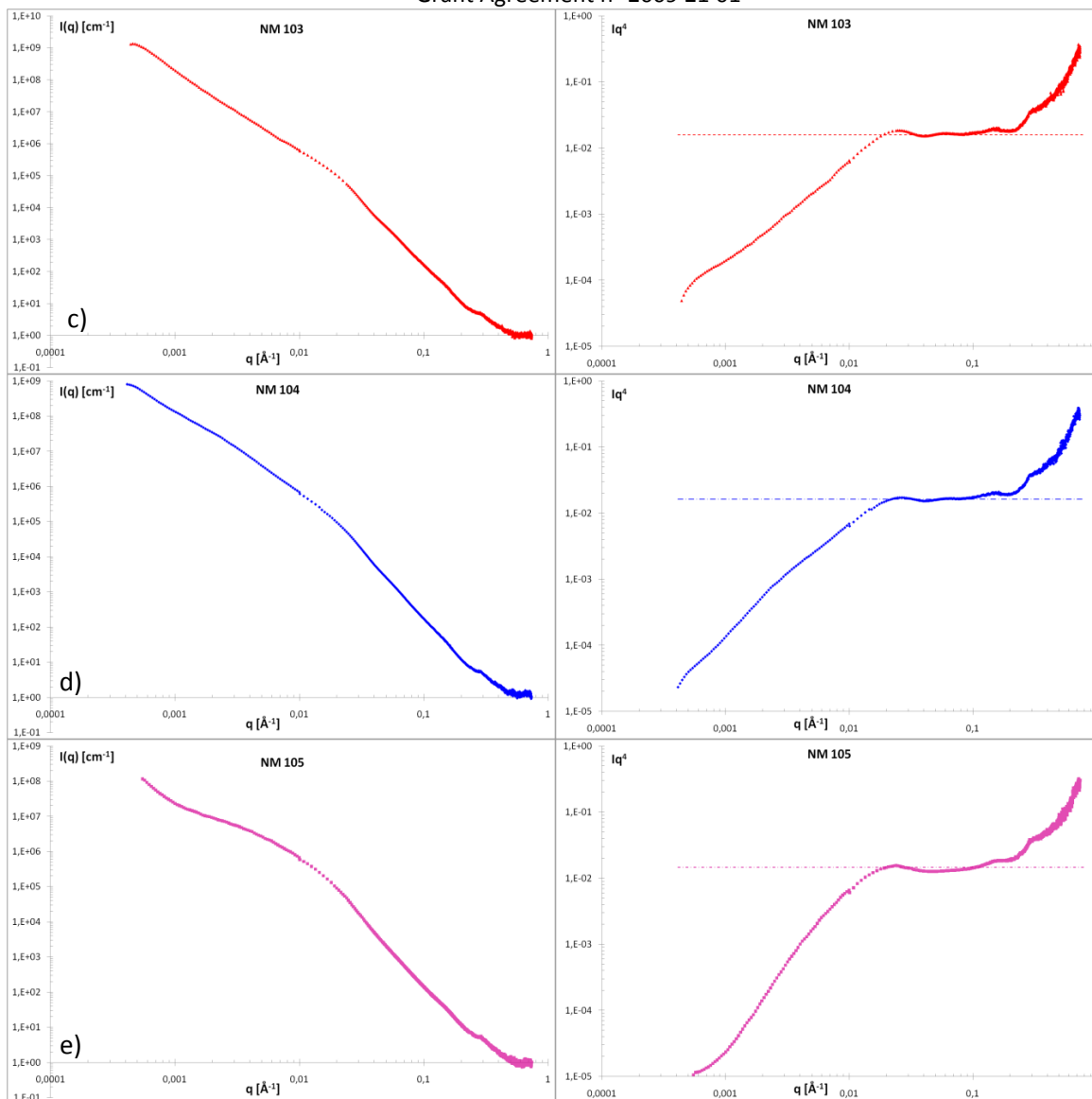


Figure 4.3: SAXS and USAXS results for  $\text{TiO}_2$  raw powders of a) NM101; b) NM102; c) NM103; d) NM104 and e) NM105.  $I(q)$  representations on the left;  $I(q)q^4$  representation revealing Porod's plateaus on the right.

It should be noted that each NM displays a specific curve, revealing different nanostructures of those materials (except for NM103 and NM104 which are morphologically identical and differ only from their organic coating). Therefore, it is possible to discriminate between nanomaterials which may display similar aggregate size in suspension, when studied by other techniques such as dynamic light scattering for example.

The calculation results for specific surface area of  $\text{TiO}_2$  powders, expressed in  $\text{m}^{-1}$  and in  $\text{m}^2/\text{g}$ , together with uncertainty estimations, are gathered in the following table. The diameter calculated in the last column corresponds to the size of dense, perfectly monodisperse and spherical  $\text{TiO}_2$  nanoparticles that would exhibit the same mean surface area.

Table 2: Specific surface area results for TiO<sub>2</sub> powders from SAXS measurements.

Sample	Lim Iq <sup>4</sup> [10 <sup>-3</sup> . cm <sup>-1</sup> . Å <sup>-4</sup> ]	Σ [m <sup>-1</sup> ]	Specific surface area [m <sup>2</sup> /g]	error on plateau	+ 5% error on density	Equivalent diameter for spheres [nm]
NM101	52.7	7.17E+08	169.5	+/-8.5	+/-25.4	8
NM102	20.4	2.78E+08	65.6	+/-3.3	+/-9.8	22
NM103	15.9	2.16E+08	51.1	+/-1.8	+/-6.9	28
NM104	16.3	2.22E+08	52.4	+/-2.1	+/-7.3	27
NM105	14.6	1.99E+08	47.0	+/-2.3	+/-7.0	30

#### 4.1.2 SiO<sub>2</sub> nanomaterials (NM20X)

All SAXS diffractograms and the corresponding representations in I(q)q<sup>4</sup> for SiO<sub>2</sub> powders are displayed in Figure 4.4

The diffractograms for the different SiO<sub>2</sub> nanomaterials are very much alike, which indicates that their nanostructures are very close in terms of size and shape of the nanoparticles.

On NM204 curve, some oscillations appear, revealing that this material is less polydisperse than the others. A general rule specify that for spherical particles of radius R, the first oscillation stands at  $qR = 4.5$ . For the NP radius estimation of 21 nm, this corresponds to  $q=0.043 \text{ \AA}^{-1}$ , which is indeed the position of the first oscillation observed on NM204 curve.

The calculation results for specific surface area of SiO<sub>2</sub> powders, expressed in m<sup>-1</sup> and in m<sup>2</sup>/g, together with uncertainty estimations, are gathered in Table 3. The diameter calculated in the last column corresponds to the size of dense, perfectly monodisperse and spherical SiO<sub>2</sub> nanoparticles that would exhibit the same mean surface area.

 Table 3: Specific surface area results for SiO<sub>2</sub> powders from SAXS measurements.

Sample	Lim Iq <sup>4</sup> [10 <sup>-3</sup> . cm <sup>-1</sup> . Å <sup>-4</sup> ]	Σ [m <sup>-1</sup> ]	Specific surface area [m <sup>2</sup> /g]	error on plateau (m <sup>2</sup> /g)	+ 5% error on density (m <sup>2</sup> /g)	Equivalent diameter for spheres [nm]
NM200	5.6	2.71E+08	123.3	+/-4.9	+/-17.3	22
NM201	5.2	2.71E+08	123.3	+/-8.3	+/-20.6	22
NM202	7.8	4.04E+08	184.0	+/-17.8	+/-36.2	15
NM203	8.0	3.67E+08	167.2	+/-13.4	+/-30.1	16
NM204	6.3	2.89E+08	131.7	+/-22.9	+/-36.1	21

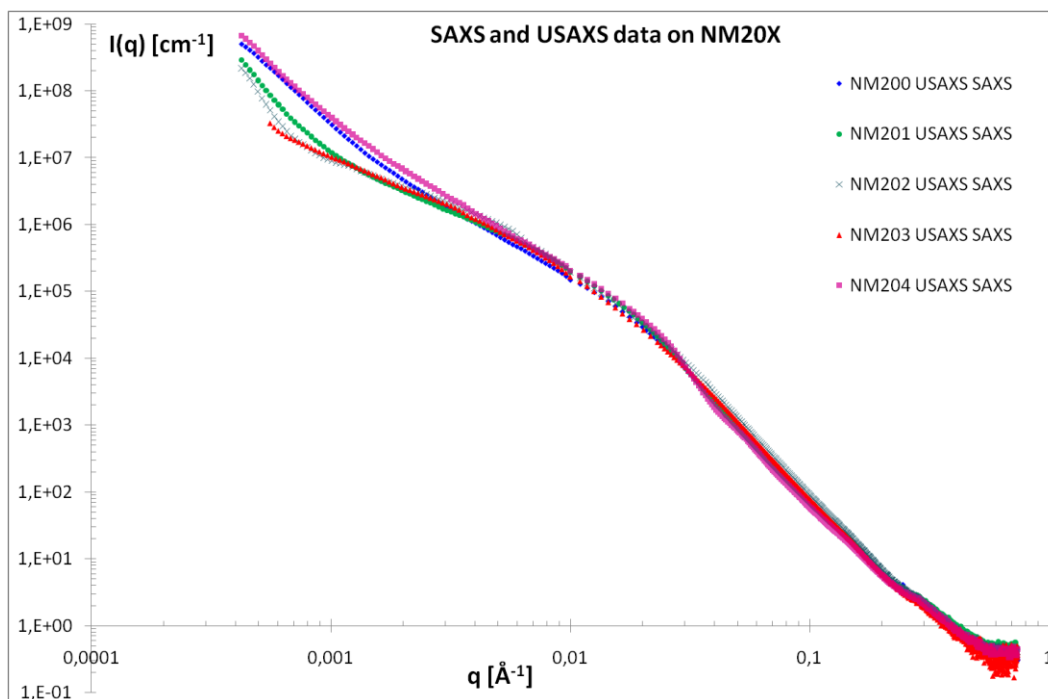


Figure 4.4: SAXS and USAXS results for  $\text{SiO}_2$  raw powders NM200 (blue diamonds), NM201 (green circles), NM202 (blue crosses), NM203 (red triangles) and NM204 (pink squares).

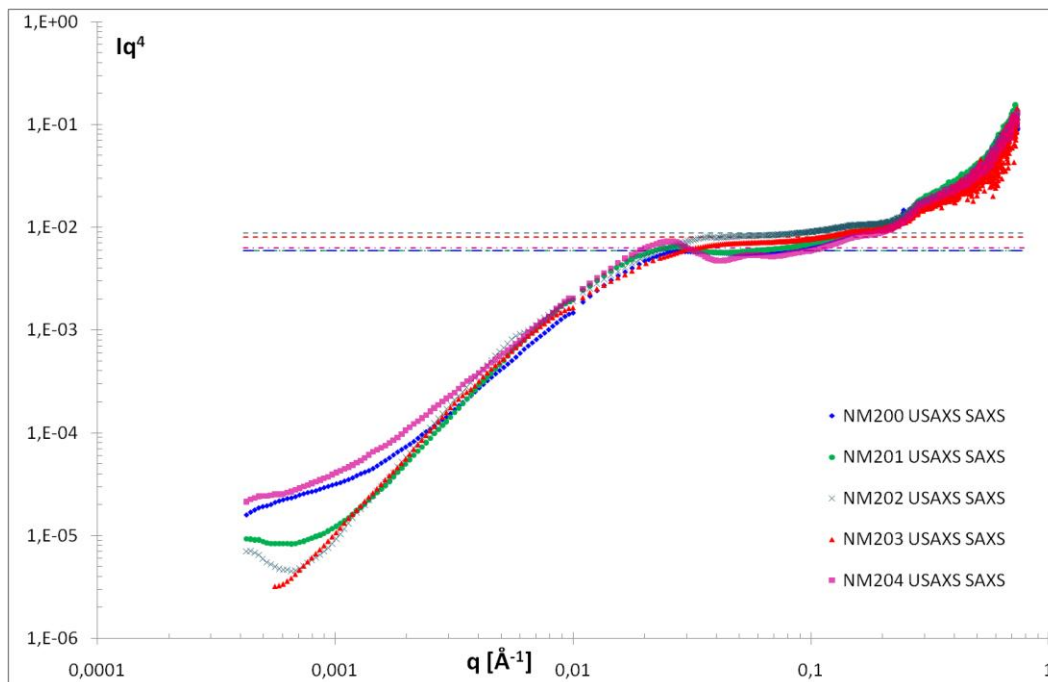
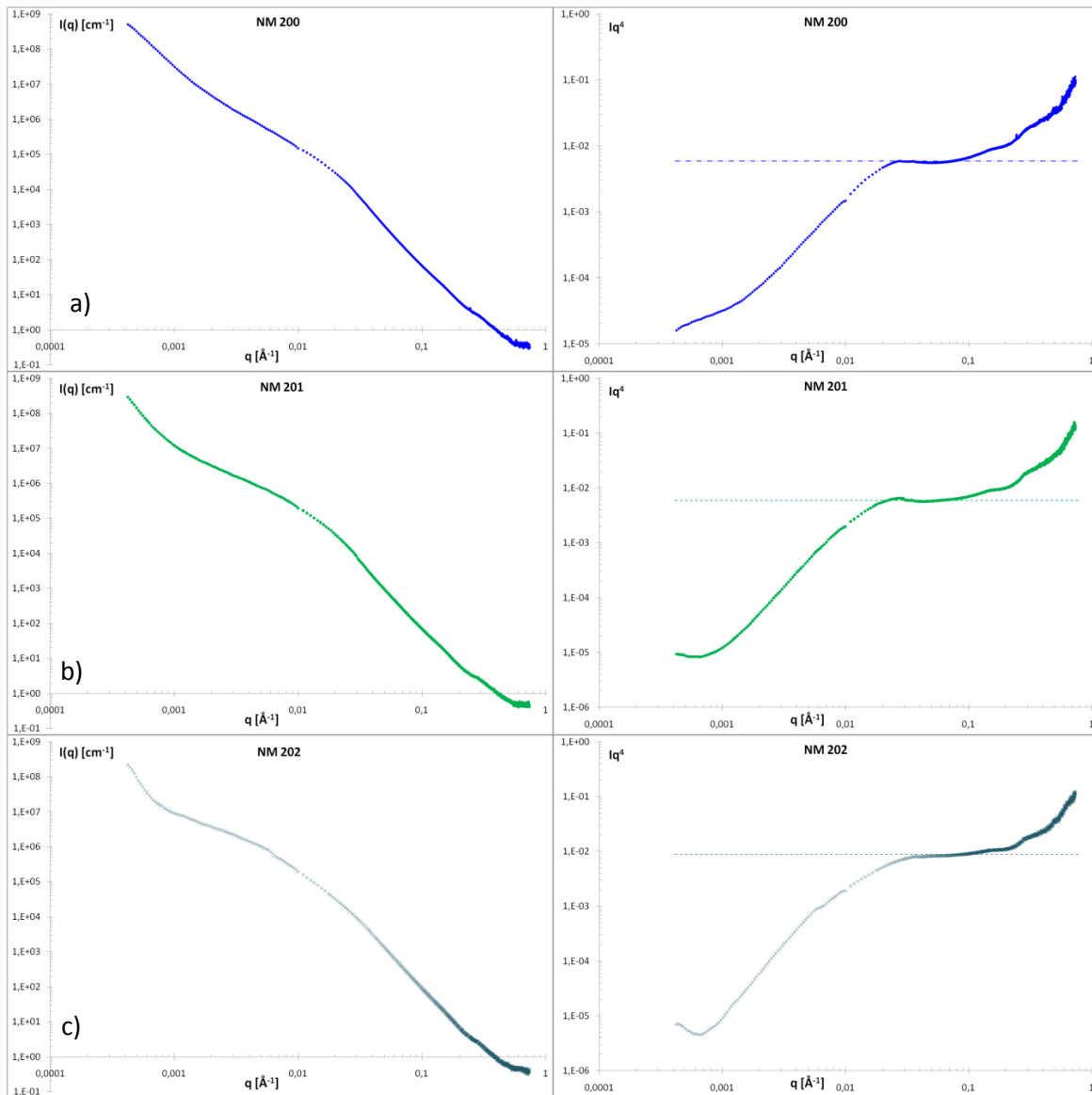


Figure 4.5: Representation in  $Iq^4$  of SAXS and USAXS results of NM200 (blue diamonds), NM201 (green circles), NM202 (blue crosses), NM203 (red triangles) and NM204 (pink squares). The dotted lines are the corresponding Porod's plateaus.



d)

c)

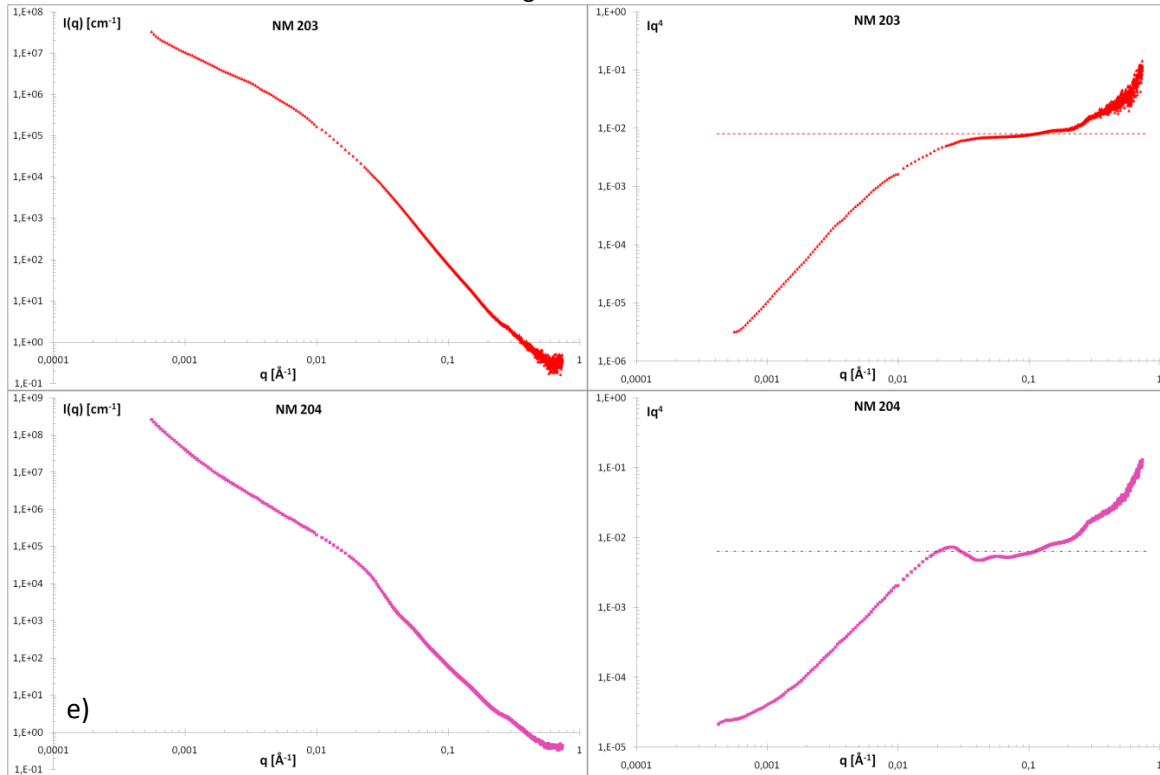


Figure. 4.6: SAXS and USAXS results for  $\text{SiO}_2$  raw powders of a) NM200; b) NM201; c) NM202, d) NM203 and e) NM204.  $I(q)$  representations on the left;  $I(q)q^4$  representation revealing Porod's plateaus on the right.

#### 4.1.3 CNT nanomaterials (NM40X)

All SAXS diffractograms and the corresponding representations in  $I(q)q^4$  for CNT powders are displayed in Figure

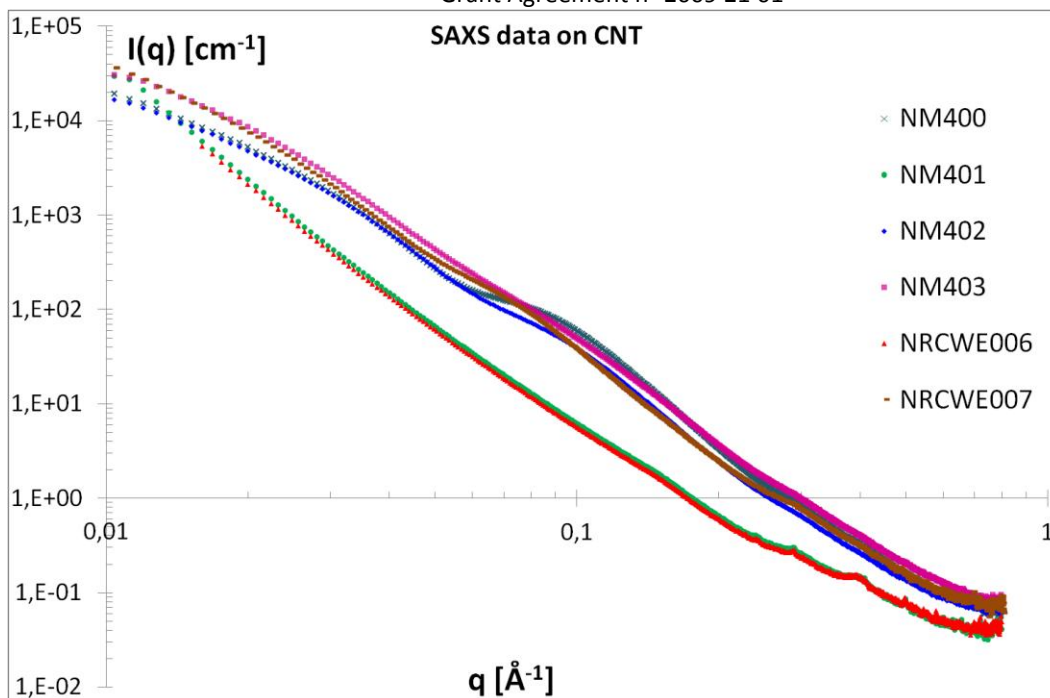


Figure 4.7: SAXS results for CNT raw powders NM400 (blue crosses), NM401 (green circles), NM402 (blue diamonds), NM403 (pink squares), NRCWE006 (red triangles) and NRCWE007 (brown bars).

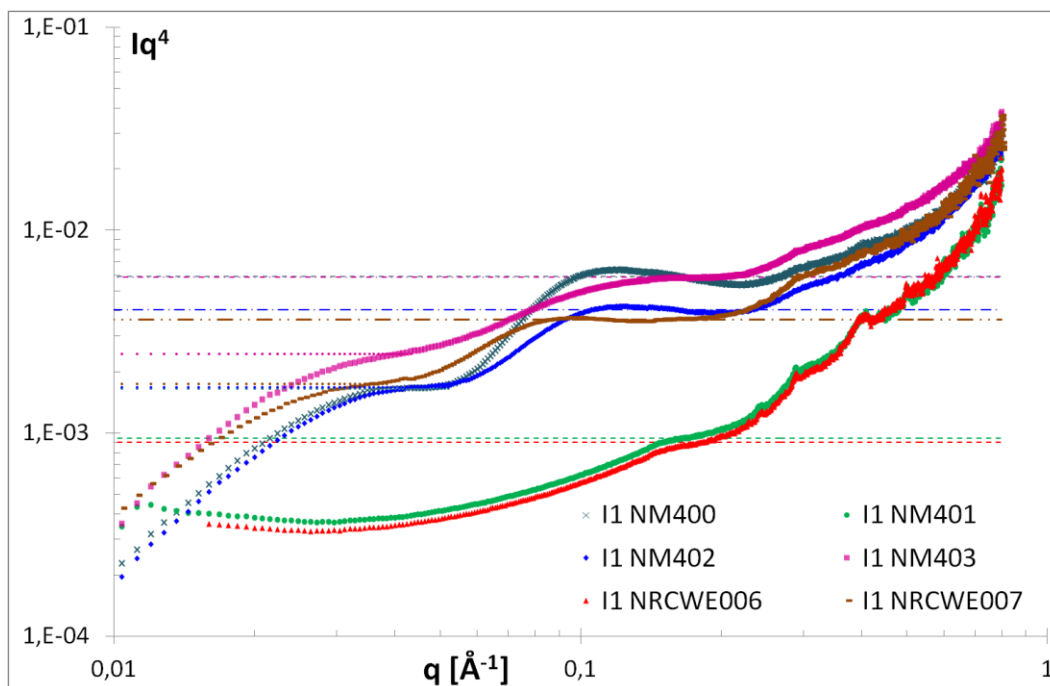
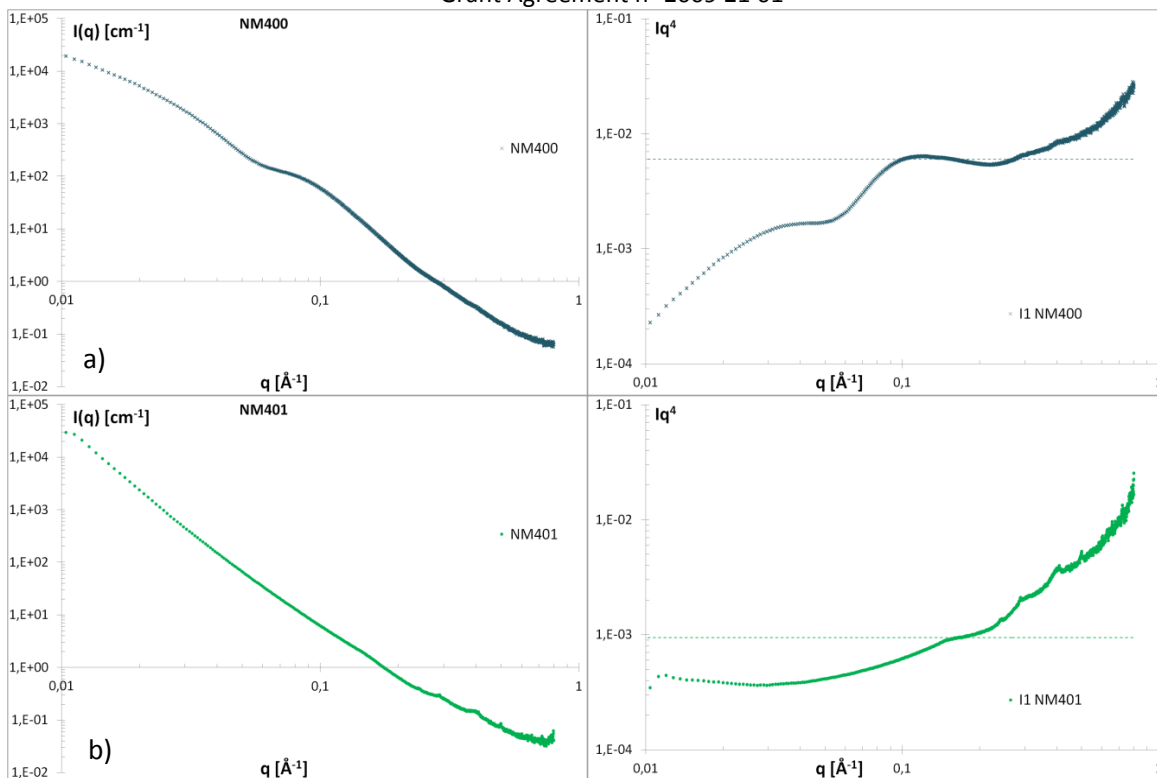
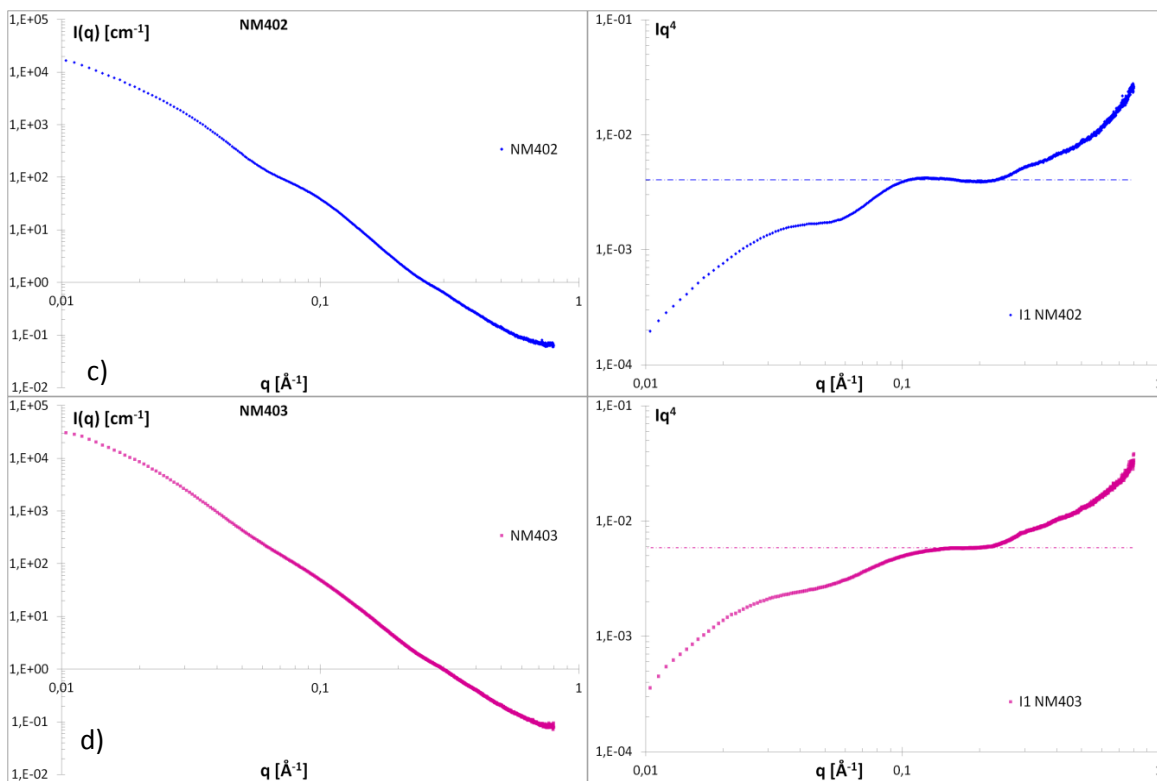


Figure 4.8: Representation in  $Iq^4$  of SAXS results of NM400 (blue crosses), NM401 (green circles), NM402 (blue diamonds), NM403 (pink squares), NRCWE006 (red triangles) and NRCWE007 (brown bars). The dotted lines are the corresponding Porod's plateaus.



Continued on next page



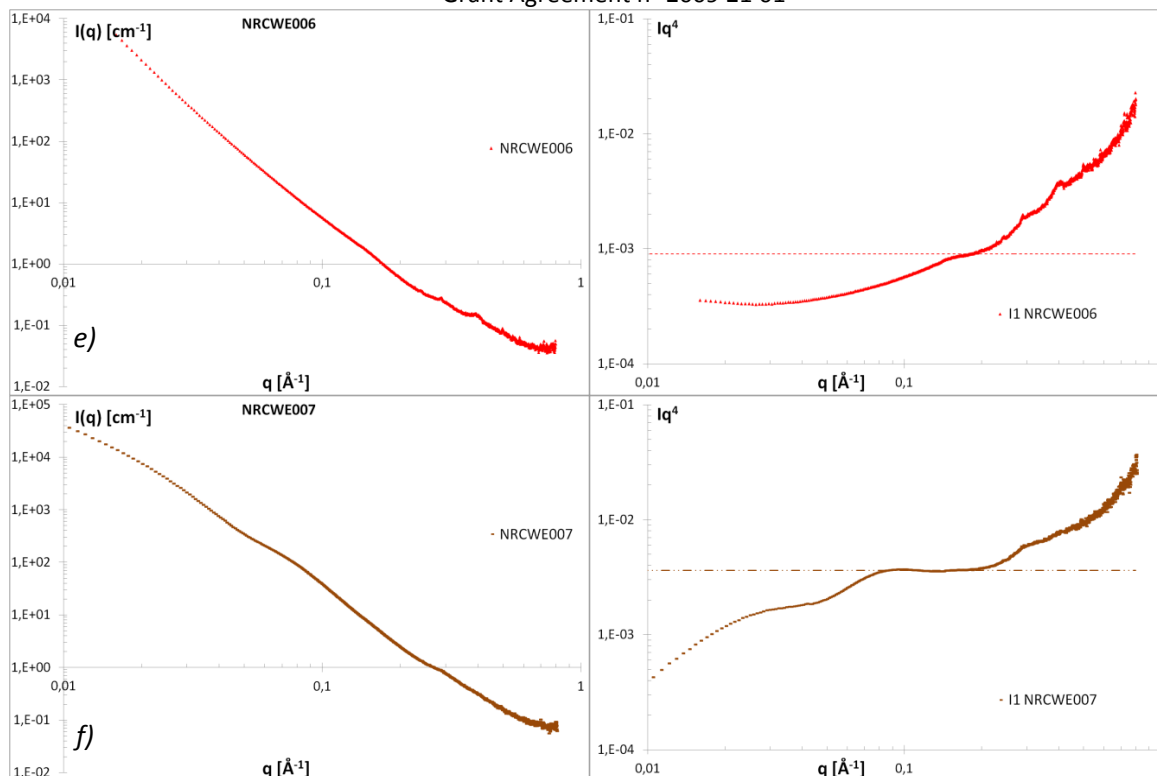


Figure 4.9 : SAXS results for CNT raw powders of a) NM400, b) NM401, c) NM402, d) NM403, e) NRCWE006 and f) NRCWE007.  $I(q)$  representations on the left;  $I(q)q^4$  representation revealing Porod's plateaus on the right.

Among carbon nanotube powders, NRCWE006 and NM401 stand out from the others and do not display any real plateau. Therefore, their specific surface area is difficult to assess, but remains very low compared to other CNTs, indicating the presence of true aggregates and/or the big nanotubes observed by TEM (see report D4.2).

Two plateaus are clearly visible for NM400, NM402, NM403 and NRCWE007. The highest plateaus reflect the presence of very small carbon nanotubes displaying high specific surface areas. The presence of another plateau for lower  $q$  indicates that, preventing there is no major contamination by any scattering impurity, carbon is arranged in some secondary structures of finite size. NM400 and NM402 seem to have a similar secondary structure, but different nanotube units (in terms of size and/or multiwall properties). For NM403, the two plateaus are less pronounced and the size difference between the primary and secondary structure is smaller.

The length of nanotubes is not accessible in the  $q$  range of the instruments used.

The calculation results for specific surface area of CNT raw powders, expressed in  $\text{m}^{-1}$  and in  $\text{m}^2/\text{g}$ , together with uncertainty estimations, are gathered in Table 9. The size calculated in the last column corresponds to the cylinder diameter of "dense" ( $1.4 \text{ g/cm}^3$ ), perfectly monodispersed carbon nanotubes of infinite length that would exhibit the same mean surface area.

The order of magnitude of the secondary structures present in NM400, NM402, NM403 and NRCWE007, can be estimated from the height of the lower plateaus, assuming a spherical shape. Values are reported in Table 5.

Table 4: Specific surface area results for CNT raw powders from SAXS measurements.

Sample	$\text{Lim } Iq^4$ [ $10^{-3} \cdot \text{cm}^{-1} \cdot \text{Å}^{-4}$ ]	$\Sigma$ [ $\text{m}^{-1}$ ]	Specific surface area [ $\text{m}^2/\text{g}$ ]	error on plateau ( $\text{m}^2/\text{g}$ )	+ 5% error on density ( $\text{m}^2/\text{g}$ )	Equivalent diameter for cylinders [nm]
NM400	5.9	2.65E+08	189.3	+/-8.1	+/-27.1	15
NM401*	0.9	4.27E+07	> 30.5	+/-1.5	+/-4.6	< 94
NM402	4.0	1.82E+08	130.3	+/-4.2	+/-17.2	22
NM403	5.9	2.65E+08	189.0	+/-10.8	+/-29.7	15
NRCWE006*	0.9	4.07E+07	> 29.1	+/-1.5	+/-4.4	< 98
NRCWE007	3.6	1.64E+08	116.9	+/- 2.5	+/-14.1	24

\*For NM401 and NRCWE, no real plateau is observed so the surface area calculation is only a minimum estimation.

Table 5: Values obtained from the lower plateaus observed for NM400, NM402, NM403 and NRCWE007, and derived typical size of secondary structures.

Sample	low plateau [10 <sup>-3</sup> . cm <sup>-1</sup> .A <sup>-4</sup> ]	$\Sigma$ [m <sup>-1</sup> ]	Specific surface area of secondary structure[m <sup>2</sup> /g]	Estimation of secondary structure size (spherical assumption) [nm]
NM400	1.65	7.45E+07	53.2	54
NM402	1.68	7.59E+07	54.2	53
NM403	2.45	1.11E+08	79.0	36
NRCWE007	1.75	7.90E+07	56.5	51

## 4.2 BET

The results on the specific surface area, pore volume and microporosity of the MN is summarized in Table 6. In addition to data generated directly by the NANOGENOTOX partners, two additional data were obtained in the MWCNT samples NRCWE-006 and NRCWE-007. There appears to be a major difference between the two data on NRCWE-006.

Table 6: Summary of BET results on all three test materials and the internal reference.

Material	BET surface	Total pore volume	Micro surface area	Micropore volume
	m <sup>2</sup> /g	ml/g	m <sup>2</sup> /g	ml/g
ZnO	10.037	0.0319	0.0	0.0
NM100	9.230	0.0324	0.0	0.0
NM101	316.07	0.3190	13.625	0.00179
NM102	77.992	0.2996	1.108	0.00034
NM103	50.835	0.2616	0.0	0.0
NM104	56.261	0.1935	0.0	0.0
NM105	46.175	0.1937	0.0	0.0
NM200	189.16	0.7905	30.044	0.01181
NM201	140.46	0.5815	23.144	0.00916
NM202	204.11	0.5136	8.268	0.00084
NM203	203.92	0.4991	5.332	0.0
NM204	136.60	0.5057	17.485	0.00666

Continued on next page

NM400	254.00	0.9613	0.0	0.0
NM401	17.850	0.0776	0.0	0.0
NM402	226.39	0.8892	15.747	0.00814
NRCWE-006 (MWCNT)	74.911	0.3212	9.431	0.00614
NRCWE-006	22.0*			
NRCWE-007	180.0*			

\* Data obtained in the EU FP7 NANODEVICE project as a commercial service from QUANTACHROME GmbH & Co. KG ([6] Birkedal et al., 2012).

#### 4.2.1 TiO<sub>2</sub> (NM10X)

For TiO<sub>2</sub> nanomaterials (except for NM102) BET was straightforward and data treatment produced very good correlation coefficients. NM102 is photocatalytic anatase and thus the initial desorption may lead to some changes. Nevertheless, the result of NM102 surface area from producers and the one obtained by us are quite similar (90 vs 78 m<sup>2</sup>/g). The nitrogen adsorption isotherms are plotted in Figure 14.

#### 4.2.2 Synthetic Amorphous Silica (NM20#)

Figure 15 shows the nitrogen adsorption isotherm for all SAS samples. The curves suggest that all SiO<sub>2</sub> NM have the same comportment.

#### 4.2.3 Carbon nanotubes (NM40#)

Figure 16 shows the nitrogen adsorption isotherm for all MWCNT samples. The isotherms of nitrogen sorption experiments for carbon nanomaterials for NM 400, 401 and 401 are similar to those of SiO<sub>2</sub> materials. However, the data from NRCWE-006 (MWCNT) isotherm is not as good. The results may be due to the presence of extremely volatile compounds in that sample.

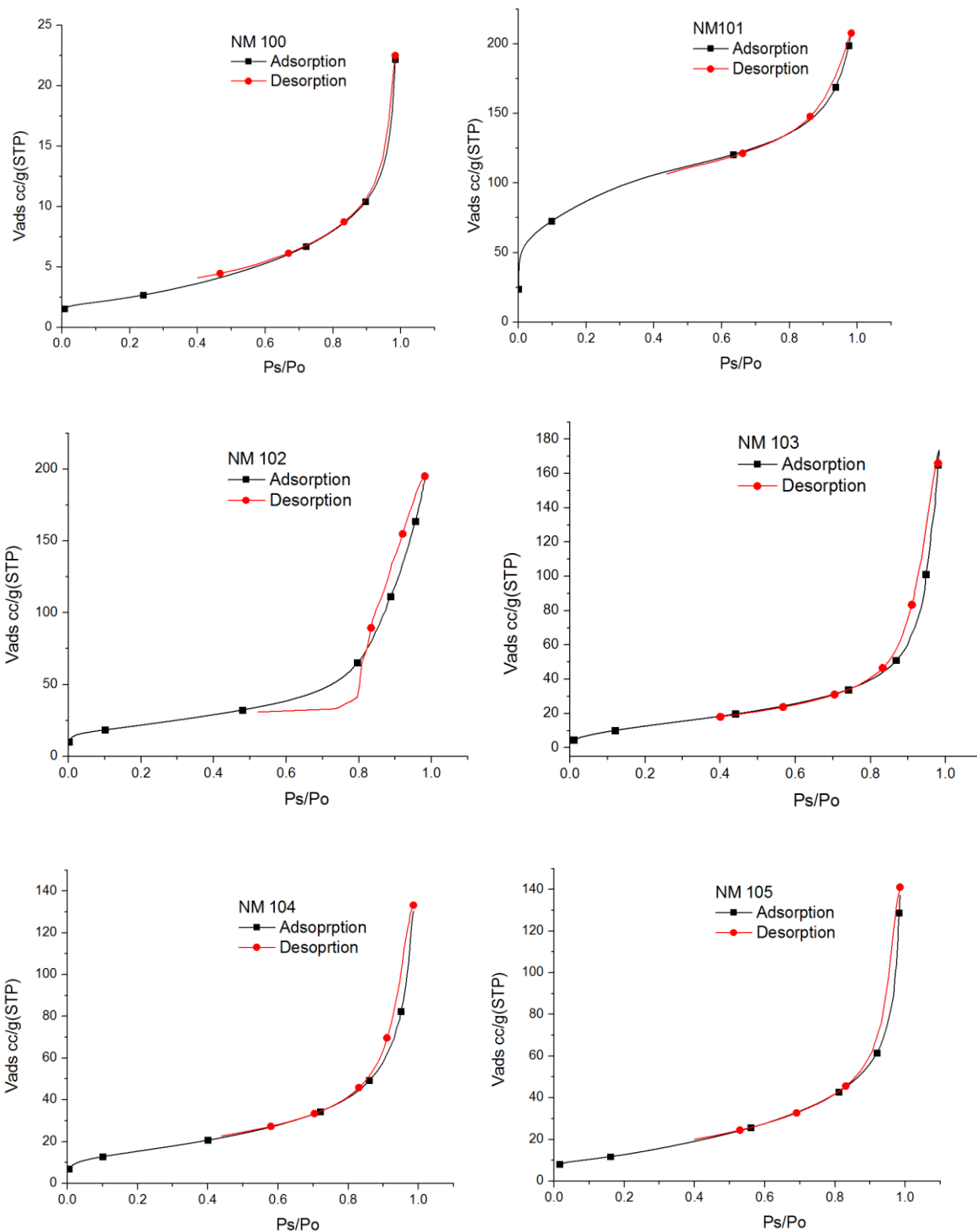


Figure 4.10: Isotherms of nitrogen sorption experiments at 77K for the  $\text{TiO}_2$  nanomaterials. The sample numbers are mentioned in the title of each plot.

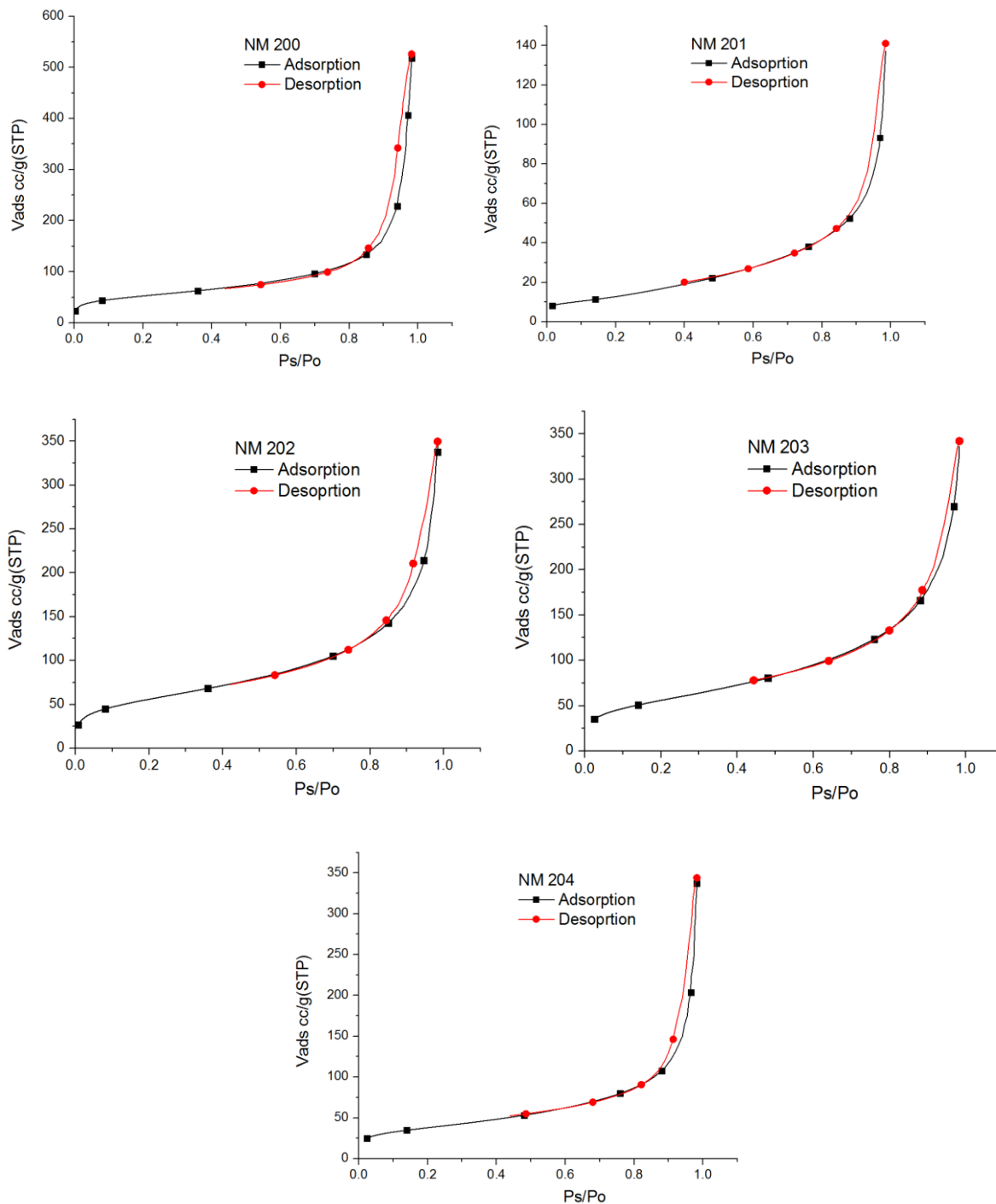


Figure 4.11: Isotherms of nitrogen sorption experiments at 77K for SiO<sub>2</sub> nanomaterials. The sample numbers are mentioned in the title of each plot.

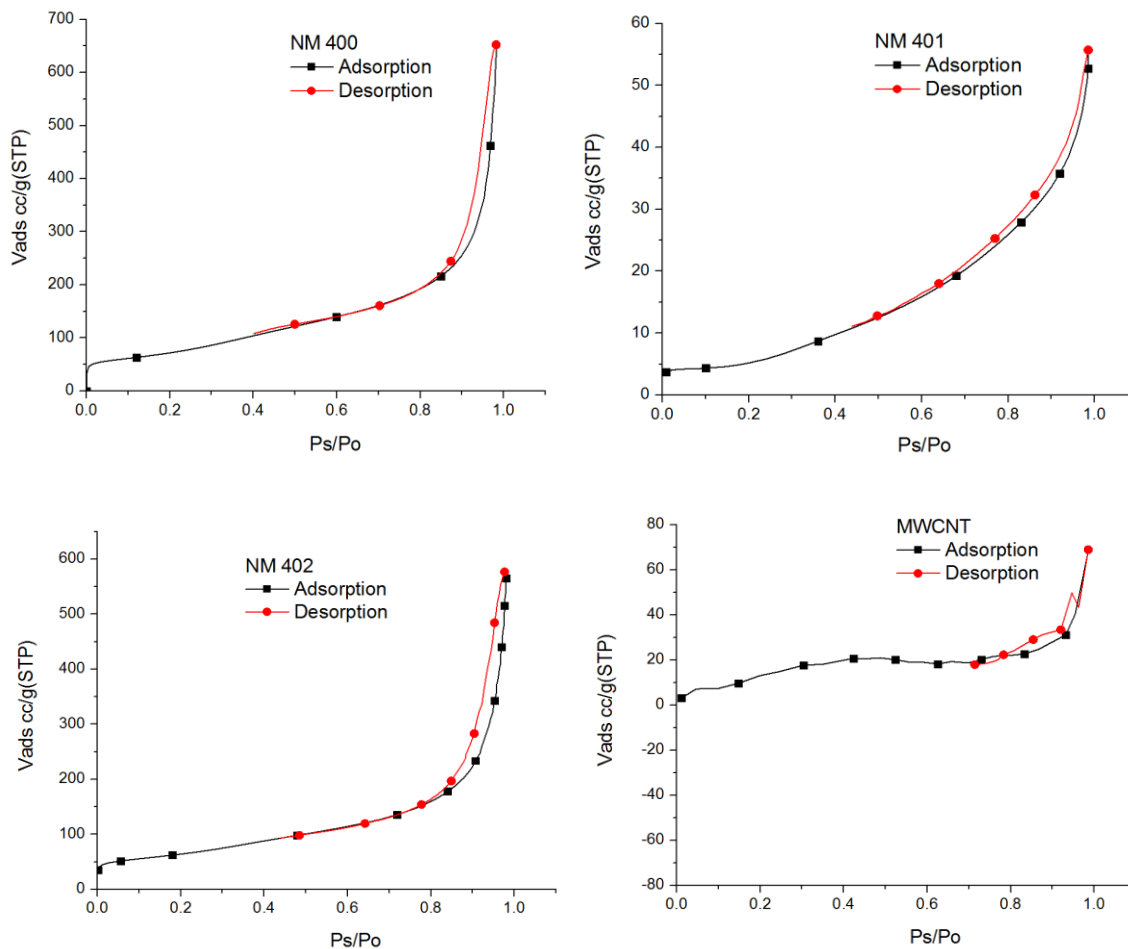


Figure 4.12: Isotherms of nitrogen sorption experiments at 77K for carbon nanomaterials

## 5 Discussion

The results from both analytical methods show a wide range in specific surface area of the different MN samples (see summary in Table 7).

### 5.1 Comparison of SAXS and BET data obtained from the project

Comparison between the SAXS and BET data shows a relatively large difference for some of the materials. One of the greater differences were observed for NM101 where the SAXS and BET data are 169.5(+/- 8.5) and 316.07(+/- 8.1) m<sup>2</sup>/g, respectively. Hence, the value obtained from the BET model is twice that of the SAXS. This ratio is in good agreement with the general linear regression curve showing an overall average ratio of 0.55 (R<sup>2</sup> = 0.82) between the SAXS and BET data (Figure 5.1a). However, a linear relationship with a ratio of 0.85 (R<sup>2</sup> = 0.85) could be established until ca. 130 m<sup>2</sup>/g, which cover all three types of MN. The best overall data fit is reached using a power-function which give and R<sup>2</sup> of 0.92 (Figure 5.2b). Still, some uncertainty is related to the potential inhomogeneity of the powders.

Table 7: Summary of the specific surface area data obtained by BET and SAXS

Material	BET specific surface area	SAXS surface
	m <sup>2</sup> /g	m <sup>2</sup> /g
ZnO	10.037	
	<b>TiO<sub>2</sub></b>	
NM100	9.230	-
NM101	316.07	169.5(8.5)
NM102	77.99	65.6(3.3)
NM103	50.835	51.1(1.8)
NM104	56.261	52.4(2.1)
NM105	46.175	47.0(2.3)
	<b>SiO<sub>2</sub></b>	
NM200	189.16	123.3(4.9)
NM201	140.46	123.3(8.3)
NM202	204.11	184.0(17.8)
NM203	203.92	167.2(13.4)
NM204	136.60	131.7(22.9)

Continued on next page

Carbon nanotubes		
NM400	254.00	189.3(8.1)
NM401	17.850	> 30.5**(1.5)
NM402	226.39	130.3(4.2)
NM403	-	189.0(10.8)
NRCWE-006	22.0*	>29.1(1.5)**
NRCWE-007 (MWCNT)	74.911	116.9(2.5)**
NRCWE-007	180.0*	

\* Data obtained in the EU FP7 NANODEVICE project. There is poor reproducibility for the NRCWE-007 with the Nanodevice project value. \*\* For NM401 and NRCWE, no real plateau is observed in SAXS, so the surface area calculation is only a minimum estimation.

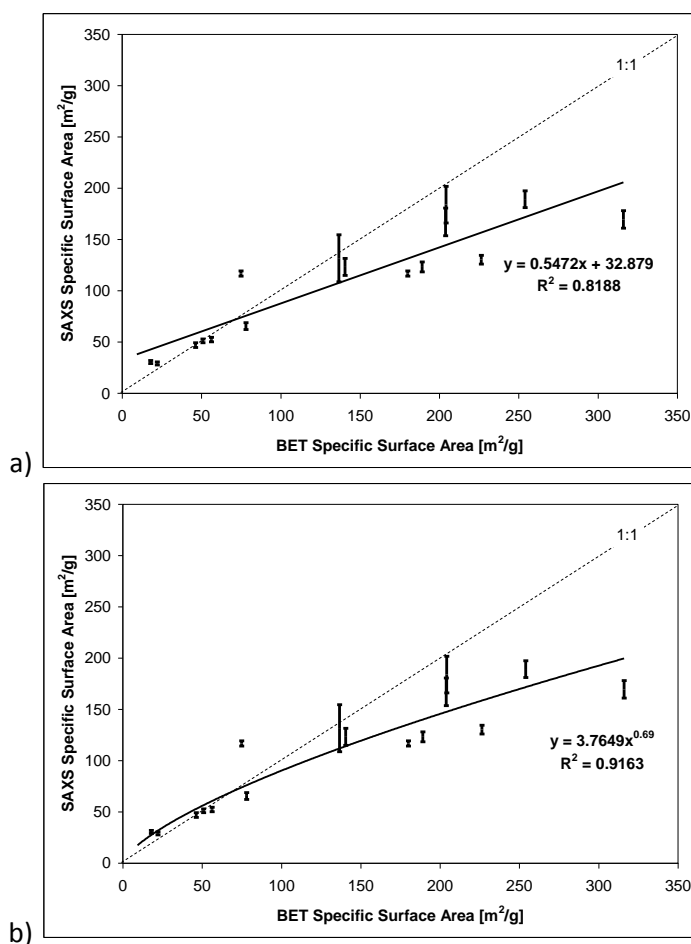


Figure 5.1: Plot of SAXS specific surface area data plotted against the BET specific surface area data. All data listed in Table 12 are included.

Assessed from the methodology, most of the differences may be explained by the combined errors in density and placement of plateau. Other explanations may come from the difference in thermal treatment and outgassing of the powders before BET analysis. Indeed, thermogravimetric analysis showed a loss of 8 and 2 wt% in the analysis of NM101 and NM200, respectively, which could come from organic coating or water, “wrapping” the nanoparticles and therefore responsible for a decrease of the X-ray contrast and subsequently of the specific surface area seen by SAXS.

It should also be mentioned that the Porod plateau is determined in a  $q$  range up to  $0.3 \text{ \AA}^{-1}$ , which corresponds in the direct space to dimensions down to 2 nm. This means that it is very difficult to estimate a roughness smaller than 2 nm in these conditions (leading to an additional surface area). This could explain why, in BET measurements,  $N_2$  molecules, smaller than 2 nm, might “see” more surface in general.

Both of these issues would have greatest importance on the high-surface area nanomaterials.

## 5.2 Comparison between BET data obtained from the project and BET data from producers

The results from the BET analyses conducted in the project are compared with manufacturers data in Tables 12-14. It is evident that the values obtained in the project are in good agreement with the producer provided values for  $TiO_2$  and silica. Unfortunately for carbon nanomaterials (NM40X) there is not enough data to attempt a meaningful correlation. The values for NM400 are similar, however the value for NM401 is below the very broad range of 40-300  $m^2/g$  provided by the producer. Overall, the comparability between reported and measured BET surface area data is good (Figure 18). Only 2 or 3 serious outliers were observed of which the one related to NM401 may be due to sample inhomogeneity.

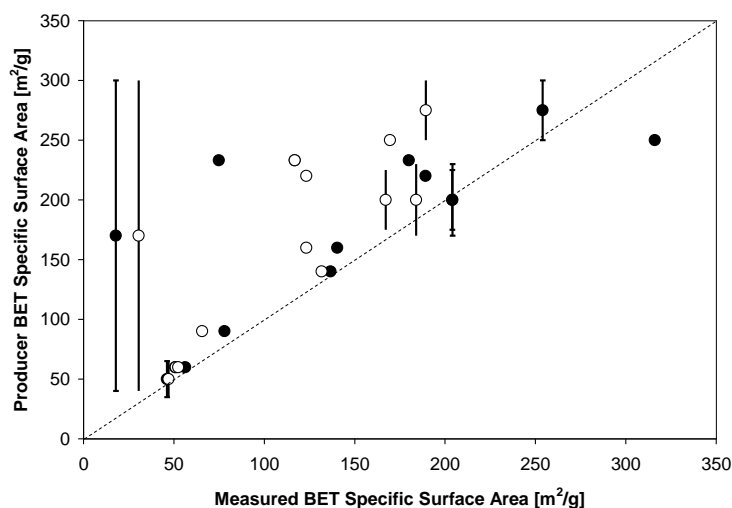


Figure 5.2: Plot of measured BET (filled spheres) and SAXS (open spheres) specific surface area data plotted against the BET specific surface area data reported by the producers. Generally good agreement is observed between measured and producer data. As discussed above, SAXS data appears to underscore the BET surface areas at high surface area values.

Table 8: Comparison of obtained BET data with the provided from producers for TiO<sub>2</sub>.

JRC Code	Phase	Purity wt%	BET (m <sup>2</sup> /g) producer	impurity / coating	SAXS (m <sup>2</sup> /g) CEA	BET (m <sup>2</sup> /g) IMC-BAS
NM-100	anatase	98.5	-	-	-	9.230
NM-101	anatase	91(99)*	>250	9%*	169.5(+/-8.5)	316.07
NM-102	anatase	95	90	-	65.6(+/-3.3)	77.992
NM-103	rutile	89	60	Al <sub>2</sub> O <sub>3</sub> 6%, silicone - Dimethicone 2%	51.1(+/-1.8)	50.835
NM-104	rutile	90	60	Al <sub>2</sub> O <sub>3</sub> 6% - Dimethicone 2%	52.4(+/-2.1)	56.261
NM-105	rutile/anatase	-	50+/-15	-	47.0(+/-2.3)	46.175

 Table 9: Comparison of obtained BET data with the provided from producers for SiO<sub>2</sub>.

JRC Code	Special notes	Purity wt%	BET (m <sup>2</sup> /g) producer	impurity / coating	SAXS (m <sup>2</sup> /g) CEA	BET (m <sup>2</sup> /g) IMC-BAS
NM-200	PR-A-02	-	220	10 SiO <sub>2</sub> 1 H <sub>2</sub> O, 2% soluble salts	123.3(+/-4.9)	189.16
NM-201	PR-B-01	-	160	10 SiO <sub>2</sub> 1 H <sub>2</sub> O, 1,5% soluble salts	123.3(+/-8.3)	140.46
NM-202	PY-AB-03	>99,8	170-230	-	184.0(+/-17.8)	204.11
NM-203	PY-A-04	-	200+/-25	hydrates?	167.2(+/-13.4)	203.92
NM-204		-	140	-	131(+/-22.9)	136.60

Table 10 Comparison of obtained BET data with the provided from producers for CNT.

JRC Code	Phase	CNT tube length	BET (m <sup>2</sup> /g) producer	impurity / coating	SAXS (m <sup>2</sup> /g) CEA	BET (m <sup>2</sup> /g) IMC
NM-400	MWCNT	~1.5 um long	250-300	10 wt% oxides/coated with pyrogenic carbon	189.3(+/-8.1)	254.0
NM-401	MWCNT	5-15 um long	40-300	~2% amorph. carbon	30.5*(+/-1.5)	17.9
NM-402	MWCNT	0.1-10 um long	-	<10 wt%	130.3(+/-4.2)	226.4
NM-403	MWCNT	1->10 µm long	-	-	189.0(+/-10.8)	-
NRCWE-006	MWCNT	segments; 3-5 um long	-		29.1*(+/-1.5)	74.9/22.0*
NRCWE-007	MWCNT	8-15 nm OD; 10-50 um long	233	ca. 3.2 wt% C impurities/ < 1.5wt% ash (Al, Cl, S)	116.9(+/-2.5)	180.0*

\* Data obtained in the EU FP7 NANODEVICE project as a commercial service from QUANTACHROME GmbH & Co. KG ([6] Birkedal et al., 2012).

## 6 Conclusions

The samples were analyzed for their specific surface area using BET and SAXS, which are two different analytical methods relying on nitrogen gas adsorption and X-ray scattering, respectively.

The results show a wide range in the specific surface areas of the MN analyzed with BET. One concern, however, is the great differences observed between the measurements of NRCWE-006 and NRCWE-007, which suggest a high degree of inhomogeneity.

Proof of principle has been shown for SAXS analysis of all three compounds (TiO<sub>2</sub>, amorphous silica and CNT) for the deduction of surface area is applicable. However, there is not an overall linear correlation between SAXS and BET data. A high correlation is found until ca. 130 m<sup>2</sup>/g. Hereafter, the SAXS appears to underscore the specific surface area determined by BET. In this assessment, one must also consider the differences and limits of the methods. The determination of surface area for very small (below 10nm in diameter for silica) and bigger (>200 nm) particles needs more attention.

The BET results given by producers are generally in very good agreement with the NANOGENOTOX data. This suggests that producer instrumental capacity and the SOPs for making BET analysis are similar or of same quality as the procedures used in NANOGENOTOX. All being well as SAXS data confirms the obtained results.

## References

*This report is based on the interim project reports and direct contributions from all co-authors. Most of the interim reports are available for the NANOGENOTOX consortium on the CIRCA web-page and not cited specifically in this report.*

1. Jensen K, Clausen PA, Birkedal R, Kembouche Y, Christiansen E, Levin M, Koponen I, Jacobsen N, Wallin H, De Temmeman P-J *et al*: **Standard operating procedures for characterization of the selected manufactured nanomaterials and dispersions thereof**. . In: *Standard operating procedures for characterization of the selected manufactured nanomaterials types*. Edited by Jensen KA, Thieret N; 2011.
2. Jensen KA, Kembouche Y, Christiansen E, Jacobsen N, Wallin H: **The generic NANOGENOTOX dispersion protocol**. In: *Standard Operation Procedure (SOP) and background documentation Final Protocol for producing suitable manufactured nanomaterial exposure media* Edited by Jensen KA, Thieret N; 2011.
3. Lambard J, Lesieur P, Zemb T: **A Triple Axis Double Crystal Multiple Reflection Camera for Ultra Small-Angle X-Ray-Scattering**. *J Phys I* 1992, **2**(6):1191-1213.
4. Spalla O, Lyonnard S, Testard F: **Analysis of the small-angle intensity scattered by a porous and granular medium**. *J Appl Crystallogr* 2003, **36**:338-347.
5. Brunauer S, Emmett P H & Teller E.: **Adsorption of gases in multimolecular layers**. *Journal of the American Chemical Society* 1938, **60**:309-19.
6. Birkedal R, Clausen PA, Kofoed-Sørensen V, Burdett G, and Jensen KA: **D3.2a Data report on complete physico-chemical benchmark (reference) values**. Deliverable 3.2a of the EU FP7 project NANODEVICE. Edited by KA Jensen, 2011, 31 pp.

## Appendix A: Standard Operation Procedures

### SAXS Sample preparation

All TiO<sub>2</sub> powder samples were prepared in a flattened kapton tube, mounted on a circular sample holder. The typical equivalent thickness of dense material obtained is 30 µm.

Most of the SiO<sub>2</sub> powder samples were prepared in 1.5 mm glass capillaries leading to a typical equivalent thickness of dense material with a thickness of 150 µm. The NM203 powder is very sticky and was very difficult to insert into capillaries, so it was measured in a double kapton cell.

CNT powder samples were prepared in 5 mm thick or 15 mm thick cells sealed with two sticky kapton films. NM400 and NRCWE006 are very fluffy materials and therefore require the thicker cells.

Type of cell, transmission and equivalent thickness for each sample are reported in Table 11, 12, 13 respectively for TiO<sub>2</sub>, SiO<sub>2</sub> and CNT materials.

Table 11 : Experimental parameters for TiO<sub>2</sub> powder samples

Sample	cell	$e_B$	$T_{exp}$
NM101	Flattened kapton capillary	25 µm	0.31
NM102		27 µm	0.28
NM103		23 µm	0.33
NM104		36 µm	0.18
NM105		31 µm	0.23

Table 12 : Experimental parameters for SiO<sub>2</sub> powder samples

Sample	Cell	$e_B$	$T_{exp}$
NM200	1.5 mm glass capillary	115 µm	0.41
NM201	1.5 mm glass capillary	187 µm	0.24
NM202	1.5 mm glass capillary	106 µm	0.44
NM203	double sticky kapton cell	40 µm	0.73
NM204	1.5 mm glass capillary	153 µm	0.31

Table 13 : Experimental parameters for CNT powder samples

Sample	cell	$e_B$	$T_{exp}$
NM400	two sticky kapton films (5mm cell)	745 $\mu\text{m}$	0.64
NM401	two sticky kapton films (15mm cell)	1124 $\mu\text{m}$	0.52
NM402	two sticky kapton films (5mm cell)	1190 $\mu\text{m}$	0.5
NM403	two sticky kapton films (5mm cell)	1320 $\mu\text{m}$	0.46
NRCWE006	two sticky kapton films (15mm cell)	948 $\mu\text{m}$	0.57
NRCWE007	two sticky kapton films (5mm cell)	959 $\mu\text{m}$	0.57

### **BET Sample preparation and apparatus specification**

For NANOGENOTOX materials ( $\text{TiO}_2$ ,  $\text{SiO}_2$ ,  $\text{ZnO}$ , CNT) no special preparation is required. Unless the samples are sensitive to the adsorbate gas or pressure variation no special preparation is needed. Weigh 0.1 g of the material and place it in the appropriate cell size (the volume of the sample may vary from sample to sample due to difference in density etc.).

High-speed surface area and pore size analyzer NOVA 4200e (Quantachrome) was used in our case. NOVA 4200e has four preparation ports (vacuum or flow degassing) and four analysis ports. It provides single and multi-point BET surface area with  $y$ -intercept, "C" constant, slope and correlation coefficient; up to 100 adsorption and 100 desorption isotherm points; B.J.H pore size distribution calculated from the adsorption or desorption isotherm; total pore volume and average pore radius.

BET analyzer operates by measuring the quantity of gas adsorbed onto or desorbed from a solid surface at some equilibrium vapor pressure. The data are obtained by admitting or removing a known quantity of adsorbate gas (in our case Nitrogen) into or out of a sample cell containing the solid adsorbent maintained at a constant temperature below the critical temperature of the adsorbate (at temperature of liquid Nitrogen). As adsorption or desorption occurs the pressure in the sample cell changes until equilibrium is established. The quantity of gas adsorbed or desorbed at the equilibrium pressure is the difference between the amount of gas admitted or removed and the amount required to fill the space around the adsorbent (void space).

Table 14. NOVA 4200e specifications

Performance	NOVA 4200e
Analysis stations	4
Measurement types	B.E.T., STSA, adsorption isotherm, desorption isotherm
Surface area range	0.01 m <sup>2</sup> /g to no known upper limit
Pore size range	0.35 to > 400 nm (3.5 to > 4000 Å)
Minimum pore volume	(liquid) 2.2 x 10 <sup>-6</sup> ml/g
Minimum pore volume	(STP) 0.0001 cc/g
Nitrogen	YES
Other non-corrosive gases (Ar, CO <sub>2</sub> , H <sub>2</sub> , C <sub>4</sub> H <sub>10</sub> , ect.)	YES
Preparation ports	4
Methods	Vacuum and Flow
Temperature range	ambient - 450 °C, 1 °C intervals
Accuracy	± 5 °C
Accuracy (% of span)	± 0.1
Minimum pressure (mm Hg) resolution	0.016
Minimum relative pressure P/P <sub>0</sub> (N <sub>2</sub> ) resolution	2 x 10 <sup>-5</sup>
Dimensions (WxDxH)	51 cm x 51 cm x 79 cm
Weight	36.29 kg (80 lbs.)
Electrical	100-240 V, 50/60 Hz

### Equipment needed

- BET analyzer (in our case NOVA 4200e Surface Area and Pore Size Analyzer),
- Sample cells (different volumes),
- Microweigh with accuracy of 0.1 mg or better\*,
- Weighing box,
- Fume-hood.

### Materials and chemicals

- Liquid Nitrogen,
- Nitrogen,
- weighing box,
- glove box,
- Weighing boat,
- Wet and dry wipes for cleaning,
- Steel and glass spatula's,
- Vials with nanomaterials.

\* It is recommended to follow use two- or three layers of gloves for dermal protection, glasses and mask.

## A.2. Reminder on the technique and general laws

### SAXS experiment

Small-angle X-ray scattering is a technique based on the interaction between X-rays and matter to probe the structure of materials. The processed data are the intensity of X-ray scattered by a sample as a function of angular position of a detector (Figure 5).

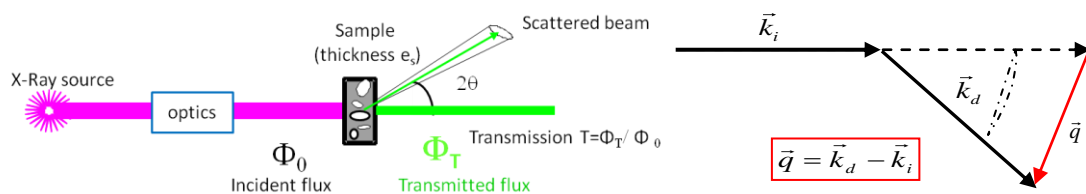


Figure A.2-1: Schematic set up for SAXS and physical quantity.

2D raw data images are converted into diffractograms displaying the **scattered intensity  $I$  as a function of scattering vector  $q$**  defined by:

$$q = \frac{4\pi \sin\theta}{\lambda} \quad \text{Eq. 3.1}$$

$\lambda$  : X-ray wavelength

Ultra small angle X-ray scattering (USAXS) measurements give access to X-ray scattering data for a smaller range of  $q$  and then complement the SAXS diffractograms. It requires a specific and very precise set-up, usually different from the one used for SAXS [3].

The intensity is expressed in **absolute scale** (in  $cm^{-1}$ ) to be independent of the experimental set up parameters (X-ray wavelength, experimental background, time of acquisition, sample thickness, etc).

General theorems of experimental physics have been developed to extract different properties of nanostructured material from the diffractograms, such as shape of nanoparticles, surface area, interactions occurring, etc.

### Porod's law

In the high  $q$  range, diffractograms display an intensity decrease in a  $q^{-4}$  trend, called the "Porod region". This region corresponds in the "real space" to the scale of the interfaces (for smooth interfaces).

Therefore, for a binary sample, the asymptotic limit of the so-called “Porod’s plateau”, when data are represented in  $Iq^4=f(q)$ , is related to the total quantity of interface  $\Sigma$  (in  $m^2/m^3$ ) between the two phases, as follows:

$$\Sigma [m^{-1}] = \frac{\lim_{\text{plateau}} (I \cdot q^4)}{2\pi(\Delta\rho)^2} \quad \text{Eq. 3.2}$$

where  $\Delta\rho$  is the difference in scattering length density between the two phases.

### *Application to powder samples*

To treat raw SAXS data and get absolute intensities, one need to normalize the intensity by the thickness of the scattering material. For powder samples where the sample thickness has no real meaning, a model system is used [4], in which we consider the effective thickness of material crossed by X-rays, called  $e_B$ , corresponding to an equivalent thickness if all the material was arranged in a fully dense (no inner or outer porosity) and uniform layer (**Erreur ! Source du renvoi introuvable.**).

The sample transmission is related to this equivalent thickness by the following equation:

$$e_B = -\frac{1}{\mu} \ln(T_{exp}) \quad \text{Eq. 3.3}$$

where  $\mu$ : material absorption coefficient for X-ray and  $T_{exp}$  is the experimental transmission (transmitted flux  $\Phi_T$ / incident flux  $\Phi_0$ ), i.e. transmission of the sample with regard to the transmission of the empty cell (kapton alone, empty capillary, etc).

A measurement is considered optimal for a transmission around 0.3. For example, the optimum thicknesses  $e_B$  for the materials studied in NANOGENOTOX are gathered in Table 2.

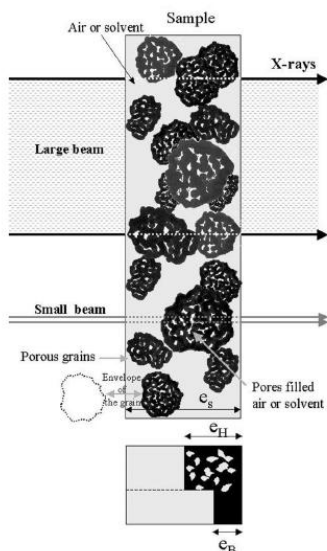


Figure A-2.2: Schematic representation of a powder sample for SAXS measurement, and definitions of equivalent thicknesses  $e_H$  and  $e_B$ .

Table 15: material properties considered and corresponding calculated optimum thickness of dense material for a sample transmission of 0.3. The absorption coefficients and scattering length density were obtained from the National Institute of Standards and Technology (NIST).

Material	density	scattering length density	absorption coefficient ( $\mu$ )	optimum thickness ( $e_B$ )
TiO <sub>2</sub>	4.23 g/cm <sup>3</sup>	3.418.10 <sup>11</sup> cm <sup>-2</sup>	470 cm <sup>-1</sup>	25 $\mu$ m
SiO <sub>2</sub>	2.196 g/cm <sup>3</sup>	1.862.10 <sup>11</sup> cm <sup>-2</sup>	77 cm <sup>-1</sup>	150 $\mu$ m
CNT	1.4 g/cm <sup>3</sup>	1.877.10 <sup>11</sup> cm <sup>-2</sup>	6 cm <sup>-1</sup>	2 mm

Specific surface areas of powders are determined on the Porod plateau using **Erreur ! Source du renvoi introuvable.** The values in m<sup>-1</sup> are then converted into m<sup>2</sup>/g taking into account the material density  $\rho_m$ :

$$\Sigma \left[ \frac{m^2}{g} \right] = \frac{\Sigma [m^{-1}]}{\rho_m \left[ \frac{g}{m^3} \right]} \quad \text{Eq. 3.4}$$

If not any uncertainty is considered for the material density, the relative uncertainty on the specific surface area calculated is directly linked to the determination of the Porod plateau:

$$\frac{\Delta \Sigma \left[ \frac{m^2}{g} \right]}{\Sigma \left[ \frac{m^2}{g} \right]} = \frac{\Delta \Sigma [m^{-1}]}{\Sigma [m^{-1}]} = \frac{\Delta [\lim(I)_1 q^4]}{\overline{[\lim(I)_1 q^4]}} \quad \text{Eq. 3.5}$$

However, if we consider a **quantifiable uncertainty on the material density**, it is passed on to the calculated **sample thickness**  $e_B$  and to the theoretical **scattering length density** of the material.

Finally, the relative uncertainty on the specific surface area is increased by the uncertainty on the material density:

$$\frac{\Delta \Sigma [m^{-1}]}{\Sigma [m^{-1}]} = \frac{\Delta [\lim(I)_1 q^4]}{[\lim(I)_1 q^4]} + \frac{\Delta \rho_m}{\rho_m} \quad \text{Eq. 3.6}$$

The uncertainty on the material density even contributes twice when the specific surface area is expressed in  $m^2/g$ :

$$\frac{\Delta \Sigma \left[ \frac{m^2}{g} \right]}{\Sigma \left[ \frac{m^2}{g} \right]} = \frac{\Delta [\lim(I)_1 q^4]}{[\lim(I)_1 q^4]} + 2 \frac{\Delta \rho_m}{\rho_m} \quad \text{Eq. 3.7}$$

All specific surface area results, together with their uncertainty calculations are presented in the next section. Errors on the Porod's plateaus have been determined manually for each diffractogram, and the uncertainty on the material density is considered to be about 5%.

## BET measurement

Surface area and porosity are important characteristics, in understanding the structure, formation and potential applications of different natural materials. For this reason it is important to determine and control them accurately. The most widely used technique for estimating surface area is the so-called BET method (Brünauer, Emmett and Teller, 1938) [5]. The concept of the theory is an extension of the Langmuir theory, which is a theory for monolayer molecular adsorption, to multilayer adsorption with the following hypotheses: (a) gas molecules physically adsorb on a solid in layers infinitely; (b) there is no interaction between each adsorption layer; and (c) the Langmuir theory can be applied to each layer.

$$c = \left( \frac{E_1 - E_L}{RT} \right) \quad \text{(eq. 3.8)}$$

Equation (1) is an adsorption isotherm and can be plotted as a straight line with  $1/v[(P_o/P)-1]$  on the  $y$ -axis and  $\phi = P_o/P$  on the  $x$ -axis according to experimental results (BET plot). The value of the slope,  $A$  and the  $y$ -intercept,  $I$  of the line are used to calculate the monolayer adsorbed gas quantity  $V_m$  and the BET constant  $C$ . The following equations can be used:

$$v_m = \frac{1}{A + I} \quad \text{(eq. 3.9)}$$

$$c = 1 + \frac{A}{I} \quad \text{(eq. 3.10)}$$

A total surface area  $S_{total}$  and a specific surface area  $S$  are evaluated by the following equations:

$$S_{BET,Total} = \frac{v_m N S}{V} \quad (eq. 3.11)$$

$$S_{BET} = \frac{S_{Total}}{a} \quad (eq. 3.12)$$

where  $v_m$  is in units of volume which are also the units of the molar volume of the adsorbate gas,  $N$  is Avogadro's number,  $S$  is the adsorption cross section of the adsorbing species,  $V$  is the molar volume of adsorbate gas,  $a$  is the mass of adsorbent (in g).



● Contact ●

**Website:**

[www.nanogenotox.eu](http://www.nanogenotox.eu)

**E-mail:**

[nanogenotox@anses.fr](mailto:nanogenotox@anses.fr)

**Coordinator:** French Agency for Food, Environmental and Occupational Health & Safety (ANSES)

27-31, avenue du Général Leclerc  
94701 Maisons-Alfort Cedex  
France



# Partners

French Agency for Food, Environmental and Occupational Health Safety (France)	<b>ANSES</b>	
Federal Institute of Risk Assessment (Germany)	<b>BfR</b>	
French Atomic Energy Commission (France)	<b>CEA</b>	
Institute of Mineralogy and Crystallography (Bulgaria)	<b>IMC-BAS</b>	
Veterinary and Agrochemical Research Centre (Belgium)	<b>CODA-CERVA</b>	
Finnish Institute of Occupational Health (Finland)	<b>FIOH</b>	
Roumen Tsanev Institute of Molecular Biology Academy of Sciences (Bulgaria)	<b>IMB-BAS</b>	
Institut national de recherche et de sécurité (France)	<b>INRS</b>	
National Health Institute Doutor Ricardo Jorge (Portugal)	<b>INSA</b>	
Scientific Institute of Public Health (Belgium)	<b>IPH</b>	
Institut Pasteur of Lille (France)	<b>IPL</b>	
Istituto superiore di sanità (Italy)	<b>ISS</b>	
The Nofer institute of Occupational Medicine (Poland)	<b>NIOM</b>	
National Research Centre for the Working Environment (Denmark)	<b>NRCWE</b>	
National Institute for Public Health and the Environment (The Netherlands)	<b>RIVM</b>	
Universitat Autònoma de Barcelona (Spain)	<b>UAB</b>	

*This document arises from the NANOGENOTOX Joint Action which has received funding from the European Union, in the framework of the Health Programme under Grant Agreement n°2009 21.*  
*This publication reflects only the author's views and the Community is not liable for any use that may be made of the information contained therein.*



Co-funded by the Health Programme of the European Union